Energy Reports 7 (2021) 1636–1650

Contents lists available at ScienceDirect

Energy Reports

journal homepage: www.elsevier.com/locate/egyr

Evaluation of thermal interface materials in mediating PV cell temperature mismatch in PV–TEG power generation

Gideon Kidegho [a,*], Francis Njoka [b,1], Christopher Muriithi [c], Robert Kinyua [d]

[a] Department of Electrical and Electronic Engineering, School of Engineering and Technology, Technical University of Mombasa, P.O. Box 90420-80100 Mombasa, Kenya
[b] Institute of Energy and Environmental Technology, Jomo Kenyatta University of Agriculture and Technology, P.O. Box 62000-00200 Nairobi, Kenya
[c] Department of Electrical & Electronic Engineering, Faculty of Engineering, Murang'a University of Technology, P.O. Box 75-10200 Murang'a, Kenya
[d] Department of Physics, College of Pure and Applied Sciences, Jomo Kenyatta University of Agriculture and Technology, P.O. Box 62000-00200 Nairobi, Kenya

ARTICLE INFO

Article history:
Received 17 October 2020
Received in revised form 14 January 2021
Accepted 14 March 2021
Available online 26 March 2021

Keywords:
Thermoelectric cooling
Temperature mismatch
Thermal interface coupling materials
PV cell mapping

ABSTRACT

Among the emerging renewable energy technologies, solar photovoltaic (PV) power generation is growing steadily in the mainstream energy supply mix contributing about 2.58% of the global total power generation by 2018 from 2.1% in 2017. The negative high PV module temperature effects continue to pose significant hurdles though being addressed through active and passive cooling methods. Thermoelectric generator (TEG) technology, given its modularity, augments well in cooling PV modules' and generating additional electricity. However, thermal coupling of the two technologies has remained an impediment to their good performance due to the microscopic roughness of the PV and TEG surfaces. Non-uniform temperature distribution from the PV cells hinders efficient heat transfer thus affecting the performance the two technologies. In this study, PV cell temperature distribution have been evaluated analytically and experimentally under outdoor setup environments. Further, cell temperatures distribution is investigated using three thermal interface materials (TIM) under air- and water-cooled environments with aluminium honeycomb cooling panels as the cooling contact medium. Results show that the three TIMs substantially reduced the temperature mismatch effects with the heat spreader (HS) presenting lower temperature and voltage mismatch compared with the other two TIMs under both air- and water-cooled test conditions exhibiting preference. Based on the best observed conditions, PV module power output increased by 1.8% and 2.5% under the two test conditions while the TEG generated an additional 19.7% and 24.85% of power, respectively. This translated to an improvement of 11.3% and 50.6%, respectively, compared to the bare cell TEG power generation. The use of TIMs hence has the potential to mitigate thermal coupling challenges associated with PV–TEG systems improving their overall power output.

1. Introduction

Power generation using solar photovoltaic (PV) technology has been on a rising growth tread and is currently a significant contributor in the mainstream electricity generation worldwide. Presently, the theoretical efficiency of a single-junction flat-plate terrestrial solar cell is limited to 30% for solar-to-electricity conversion. In their work, Greisz et al. presented a 47.1% efficient six junction III–V solar cell made using inverted metamorphic multi-junction devices (Geisz et al., 2020). With concerted research, solar PV is expected to occupy 30%–50% of the global generation by 2050 (Creutzig et al., 2017). However, the effects of high PV cell temperatures have remained a major downside to date. This is especially in the tropical and equatorial regions where the much-sought high solar irradiance is available, but subsequently accompanied with high ambient temperatures that result in heating of the solar cells (Teo et al., 2012). The electromagnetic radiation spectrum that supplies radiant energy to the PV systems consists of ultraviolet, visible light and infrared wavelengths where ultraviolet occupies 3% at 100–400 nm, visible light 44% at 400 nm–700 nm and infrared 53% at above 700 nm, of the radiant energy spectrum. The PV cell mainly absorbs the band-gap energy of visible light and part of the infrared range, while the rest above 1100 nm infrared radiant energy ends up heating the PV cell (Deng et al., 2013; Sargunanathan et al., 2016).

* Correspondence to: Institute of Energy and Environmental Technology JKUAT P.O Box 62000, NRB, Kenya.
E-mail address: kidegho.gideon@students.jkuat.ac.ke (G. Kidegho).
[1] Currently a Faculty member in the Department of Energy Technology, Kenyatta University. P.O. Box 43844-00100, Nairobi.

https://doi.org/10.1016/j.egyr.2021.03.015

Studies on the negative effects of elevated temperatures on PV cells have shown that the voltage output of a solar cell reduces by 4%–5% for every 1 °C temperature rise (Atsu and Dhaundiyal, 2019). Besides the reduction in power output, elevated cell temperatures also accelerate the cell degradation process leading to premature failure (Ferrara and Philipp, 2012). Conventional methods of installing PV modules where they are cooled by convective forces of moving air marginally improve the performance. In the tropical regions therefore, all the benefits of high irradiance are eroded by the high cell temperatures especially during the dry and hot seasons (Huld and Amillo, 2015). In such environments, Temaneh and Mukwekwe observed that a 37.8 kWp solar PV system operating at an average module temperature of 35.4 °C and ambient temperature of 25.31 °C in Namibia lost at least 3.21% of its rated system power output (Temaneh-Nyah and Mukwekwe, 2015). In studies performed to enhance solar PV cell cooling using experimental and analytical methods, it was observed that both passive and active cooling techniques can reduce the rate of increase of heating of the PV cell (Sargunanathan et al., 2016). To alleviate these negative effects associated with elevated cell temperatures, thermoelectric generator (TEG) technology becomes appropriate for absorbing the infrared-generated heat that is dissipated by the PV cells and in turn use it to generate electricity.

In his studies, Van Sark showed that the efficiency of a PV–TEG system could be improved by between 8% to 23% using thermoelectric materials (TEM) with a figure of merit, Zt of 1, and further improvements could be achieved when the cold side temperature of the TEG was maintained at 25 °C (van Sark, 2011). The beauty of TEG technology as a passive technique of cooling PV modules is that it makes use of the same heat flux to generate electricity, subsequently improving the entire system efficiency (R. et al., 2014). However, this innovative technique of cooling PV cells has challenges in temperature distribution across the individual TEG modules that affect their performance (Bahaidarah et al., 2016). The temperature mismatch affects the operating points of the TEGs modules making them operate at different maximum power points (MPPs) hence generating different voltages (Deng et al., 2013). Our comprehensive review and to the best of our knowledge, reveal that studies on mediating temperature mismatch due to varying individual PV cell temperatures have not been carried out extensively. This temperature mismatch and good thermal coupling of PV–TEG matrices significantly affects the performance of these two technologies when operated as a hybrid. Therefore, in this study, an in-depth study of individual PV cell temperature is investigated using an analytical model analysis and experimentally through systematic cell mapping techniques under three types of thermal interface materials. These investigations of PV cell temperatures are carried out on carefully mapped 13 Wp PV modules so as to inform the design of appropriate methods of thermal coupling between the PV–TEG arrays.

2. Theoretical background

2.1. PV cell cooling and TEG cooling applications/studies

PV cell temperature is a major constraint in the cells' power output because PV cells' voltage have a negative temperature coefficient and hence reduces as the temperature increases, a phenomenon well observed from the PV cell current/voltage (I–V) curve. This feature has provoked a lot of studies on PV cell cooling using both passive and active methods to recover the energy lost under elevated cell temperatures. When TEG modules are mounted under the PV modules, they absorb the heat from the PV cell reducing the cell temperature thereby improving the power output of the PV modules. The temperature gradient so created between the hot side and the cold side of the TEG modules results in generation of voltage following the Seebeck phenomenon creating dual gains in the entire PV–TEG system. The thermal–electrical conversion efficiency of TEGs is solely dependent on the figure of merit, Zt of the thermoelectric material (TEM) used. Currently the Zt of most materials is still very low at 1.5 but there are ongoing studies to develop TEMs of higher Zt by increasing their power factor $\left(\frac{s^2}{\rho}\right)$ and reducing the thermal conductivity (k) (Kishore et al., 2017).

In their work on PV efficiency optimization using active cooling methods, Peng Z. et al. observed that a PV system with integrated cooling increased its energy output by 34.6% while the same system with cooling and hot water production from the PV cooling system, increased its energy production by an extra 72.4% (Peng et al., 2017). In a study to cool PV modules using heat spreader with cotton wick structure, Chandrasekhar M. et al. observed that the cooling setup was able to reduce the maximum cell temperature from 49.2 °C to 43.3 °C and increase the PV power yield by 14% (Chandrasekar and Senthilkumar, 2015). Elsewhere, Soliman A. M. A. et al. used a three dimensional theoretical model of a PV module coupled with a 125 mm × 125 mm, 10 mm thick heat spreader to study the effects of using the heat spreader on the performance of a PV module and they realized a 15 °C decrease in the cell temperature and a corresponding 9% power increase (Soliman et al., 2020). Abu-Rahmeh T. M. evaluated the efficiency of a PV module using different cooling methods; nano-fluids, tap water and fins and observed that cooling PV modules enhanced heat transfer and improved their electrical efficiency (Abu-Rahmeh, 2017). He also observed that among the cooling media used to cool the PV module, the nano fluid (0.04% wt TiO_2) gave the best results out of the three.

Many studies have also been carried out to investigate the features of PV–TEG systems with an intention to improve their dual power output that exploits the entire solar radiation spectrum. Belkaid et al. proposed and simulated a new hybrid PV–TEG standalone system and observed that the two technologies complemented each other very well making possible continuous production of electricity and efficiency improvement of the entire system (Belkaid et al., 2018). Soltani et al. used natural air, S_iO_2/water nano fluid, forced air and Fe_3O_4/water nanofluid to cool PV–TEG system and observed that S_iO_2/water nano fluid cooling yielded the best efficiency improvement of 3.35% followed by Fe_3O_4/water nanofluid with 3.13% (Soltani et al., 2017). Zhang J. et al. used a thermal interface material; thermal grease with a thermal conductivity of 4.2 $Wm^{-1}K^{-1}$ between a monocrystalline PV and bismuth telluride TEG coupling to enhance the power output and observed that the PV cell output increased by 14% and the TEG output increased by 60% (Zhang et al., 2020a). Soliman A. M. A. et al. in their study on the impact of using different Heat Spreader (HS) sizes, SiC nanoparticles and micro channel configurations on cooling PV–TEG systems, observed that using coolants at Reynolds (Re) numbers ranging between 5 and 100 and HS, decreases the maximum PV temperature and increases the efficiency and also the net power especially at low Re numbers (Soliman et al., 2019).

2.2. Effects of temperature mismatch on TEG performance

Though TEG technology is gaining popularity in the field of PV modules cooling to improve the system efficiency, its penetration in the field is challenged by improper thermal coupling between the heat generator (PV) and the TEG modules resulting into unsatisfactory results. A couple of studies have been conducted to investigate various aspects of temperature distribution to reduce the effects of temperature mismatch. Zhou et al. investigated the performance of tempered glass and aluminium alloy sheets as module back sheet for temperature distribution by varying their thickness and observed that Type 6061 aluminium alloy

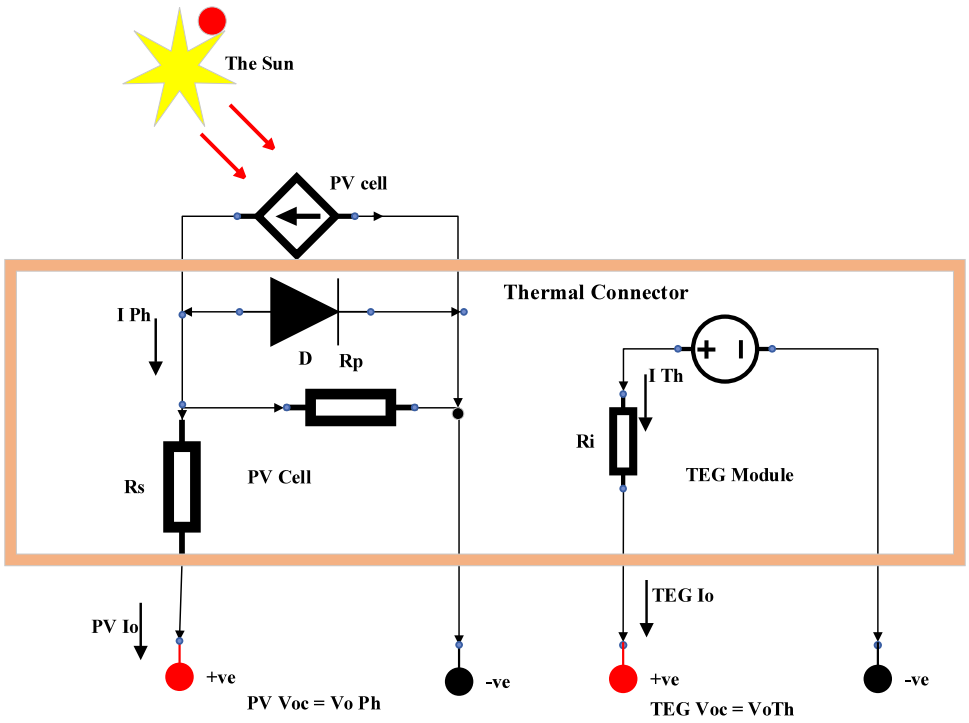

Fig. 1. A schematic of an electrical–thermal connector in PV and TEG System.
Source: Concept adopted from Fisac et al. (2014).

sheet performed better than other back sheet materials (Zhou et al., 2017). Further they also analysed a solar cell temperature distribution using a simulation model and observed that under 1000 W/m^2 irradiance, 1 m/s wind speed and 300 K ambient temperature, the temperature of the cell was highest at the centre at 331.76 K and lower along the side edges with a difference of 0.68 K and much lower at the diagonal corners with a higher difference of 1.2 K (Zhou et al., 2015). Tina G. M. et al. also conducted an experimental study to verify thermal behaviour of PV modules cells by measuring the temperature of 3 separate cells on the module and obtained a temperature difference of between 2 °C and 5 °C between the centre most cell and the outer most cell on the module (Tina and Abate, 2008).

This non-uniform distribution of temperature causes hot spots and results in reduction of efficiency and eventual structural damage due to thermal fatigue caused by thermal cycles and stresses (Royne et al., 2005). When this non-uniform cell temperature is subjected to TEG modules, they sense different hot side temperature, *Th* that directly affects the gradient, ΔT which is responsible for voltage generation (Royne et al., 2005). Tang Z. B. et al. when working on TEG electrical performance under temperature mismatch conditions observed that proper mechanical pressure on the module improves the electrical performance of the TEG and from their results, the power loss reduced from 11% to 2.4% (Tang et al., 2015). Miguel F. et al. developed a model combining the PV and TEG technologies in one semiconductor and obtained satisfactory results in increasing the efficiency of the PV–TEG under extreme temperature conditions (Fisac et al., 2014). In their study, Yin E. et al. recommended the use of adhesive TIM between the PV cell and TEG module for good thermal conductivity (Yin et al., 2017).

2.3. PV-TEG system model and governing equations

A PV module can be integrated with TEG modules using a TIM so that the two technologies can concurrently be used to generate electricity. The combined technologies can be expressed schematically as in Fig. 1 where the PV and TEG are interconnected using a common thermal connector. When the sun's radiation strikes the PV silicon cell, at 1000 W/m^2, 25 °C and AM1.5 G the cell efficiency is only 24% for monocrystalline, 19.8% for polycrystalline and 10.2% for amorphous silicon (Kasim et al., 2019). A typical polycrystalline silicon cell has an upper sensitivity boundary of $\lambda_{max} = 1110$ nm corresponding to its band gap energy, so beyond that wavelength, the spectrum results in thermal energy that adversely affects the cell (Rajkumar et al., 2015). From Fig. 1, the heat on the PV cell is then absorbed by the TEG array mounted under the cells to generate electricity following the Seebeck phenomenon. Hence the TIM or thermal connector between the PV cell and the TEG modules plays a significant role in the performance of the TEG module electricity generation process.

The operation of the TEG module as a combination of P and N semiconductor pellets is presented in Fig. 2 and used to analyse the thermo-electric operation of the TEG.

When a temperature gradient, ΔT is created between the hot side and the cold side of the TEG module, an open circuit voltage, V_{oc} is generated according to the Seebeck phenomenon and V_{oc} can be expressed as in Dousti et al. (2015) by;

$$V_{oc}TEG = \alpha_{PN}\Delta T \tag{1}$$

Where, α_{PN} are the Seebeck coefficients of the P and N semiconductor materials of the thermoelectric modules that are thermally in parallel.

The power generated by the TEG, P_{TEG} is given as (Paraskevas and Koutroulis, 2016);

$$P_{TEG} = \frac{(\alpha_{PN}\Delta T)^2}{(R_{TEG}+R_L)^2}R_L \tag{2}$$

Maximum power is obtained from the TEG when the internal resistance, R_{TEG} and the load impedance, R_L are matched and occurs at a point where V_{TEG} is equal to $\frac{V_{OC}}{2}$ and I_{TEG} is equal

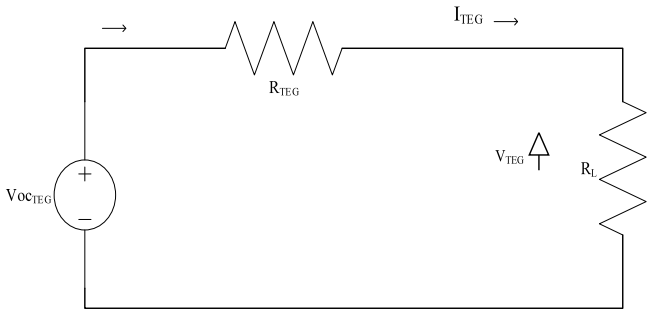

Fig. 2. A schematic of equivalent TEG Cell.

to $\frac{I_{sc}}{2}$. When the resistances R_L and R_{TEG} are matched, maximum TEG power is achieved and can be expressed as (Paraskevas and Koutroulis, 2016) ;

$$P_{TEGMax} = \frac{\alpha_{PN}^2 \Delta T^2}{4_{RTEG}} \tag{3}$$

Eq. (3) shows that the temperature gradient and hence the hot side temperature of the TEG, T_h, is key for good performance of the TEG. When T_h on the TEG modules is not uniform or near uniform, the TEGs under the PV module operate at different Maximum Power Points (MPPs) and so their generated maximum power is different even when the R_{TEG} and R_L are matched. To counter the effect of temperature mismatch, studies have been carried out by several researchers where methods of matching the Maximum Power Points (MPP) of TEGs using electronic approaches have been developed and proposed (Paraskevas and Koutroulis, 2016; Montecucco et al., 2014; Nagayoshi and Kajikawa, (2006; Dalala et al., 2018).

The main factors that influence PV cell temperature are the incident solar irradiance, ambient temperature, wind speed and the cell manufacturer's specifications on the nominal cell operating temperature (NOCT). The simplest linear expression that gives explicit correlation for the evaluation of PV temperature is where the module cell temperature T_{mod} is expressed as in Eq. (4) by Maturi et al. (2014)

$$T_{mod} = T_a + KG \tag{4}$$

The expression links T_{mod} with the ambient temperature and the incident global solar irradiance G, where K is the Ross coefficient of the module. Further, the cell temperature can be expressed as in Eq. (5) by Jakhrani et al. (2011);

$$T_c = T_a + KG_T \tag{5}$$

Where

$$K = \Delta \frac{(T_c - T_a)}{\Delta G_T} \tag{6}$$

This was further improved by Rauschenbash (1980) to take into account the effects of wind speed, heat loss coefficient and the cell nominal operating temperature as presented by Jakhrani et al. (2011);

$$T_c = T_a + \frac{G_T}{G_{TNOCT}} (T_{cNOCT} - T_{aNOCT}) \left(1 - \frac{\eta_m}{\tau_\alpha}\right) \tag{7}$$

And later, Duffie and Beckman expressed the cell temperature as Duffie and Beckman (2013);

$$T_c = T_a + \frac{G_T}{G_{NOCT}} \left(\frac{9}{5.7 + 3.8V_m}\right) (T_{cNOCT} - T_{aNOCT}) (1 - \eta_m) \tag{8}$$

And then optimized it (Duffie and Beckman, 2013) to;

$$T_c = T_a + \left[\left(\frac{G}{G_{NOCT}}\right)\left(\frac{9.5}{5.7 + 3.8V_W}\right)(T_{CNOCT} - T_{aNOCT})\left(1 - \frac{n_c}{(\tau_\alpha)}\right)\right] \tag{9}$$

3. Simulation and experimental procedures

This section comprises of analytical model development, simulations and fabrication of cell mapping techniques and temperature measurements setups. In the analytical model formulation, a model is used to analytically evaluate the PV cell temperature while in the experimental part, different setups are fabricated using various Thermal Interface Materials (TIMs) for temperature distribution and PV–TEG performance measurements.

3.1. Analytical PV cell model description

An individual PV cell on a module is a representative of the many cells on the module. A module could have 18 cells, 36 cells, 60 cells and even more and so, one of them can represent the rest on the module. The representative cell on a module is always expected to give the features and temperature of the rest of the cells because they are identical. In this study, the analysis based on the cell model provides the representative cell temperature and attempts to disclose how well the single cell temperature may represent the other cells when the actual cell temperatures are measured in the setups that follow. Previous researchers developed PV system models that have been used to predict cell temperature in different analytic and simulation platforms. The models have been mathematically explicit or implicit to suit the researcher's preferences and have also been classified as steady-state or transient approaches, where the parameters in the models are assumed to be either independent or dependent of time, respectively (Jakhrani et al., 2011). These models have been applied in many varying environments and PV mounting conditions and results of different accuracies obtained depending on the model used. Some selected models are listed in Table 1 for comparison (Jakhrani et al., 2011). Among them, the optimized Duffie and Beckman model has been applied in this study because it takes into account the cell temperature at varying wind speeds (Duffie and Beckman, 2013). The model also offers better accuracy in predicting the cell temperature and has also been preferred before by other researchers for size optimization, analysis, simulation and design of PV systems (Jakhrani et al., 2011). The Duffie and Beckman model has been used widely in designs and when compared to other models by Renata et al. the model presented the lowest average error at 5.2% (Yang et al., 2019). In this study, the analytical model analysis is performed in Microsoft excel, where input parameters such as ambient temperature, wind speed and the irradiance obtained from measured matrix temperatures taken during the preliminary setups were used. This was done to help in the validation of the results.

3.2. PV module preliminary cell mapping and temperature measurement setup

A 13 Watts peak (Wp) polycrystalline PV module of 36 cells and nominal voltage of 12 V was used to carry out the cell mapping and subsequent cell temperature measurements process. The objective of the cell mapping procedure was to categorize and investigate the actual individual cell temperature differences within the PV module when subjected to uniform solar radiation levels. The cell mapping and marking was realized by first identifying the central cells on the module, marked as matrix 1 and then from there radiating outwards to each cell position with respect to the centre as shown in Fig. 3. The next nearest matrix outwards are denoted as matrix 2 followed by other sets of matrices 3, 4 and 5 up to the outermost cells on the module designated as matrix 6.

Table 1
Illustration of models for determination of PV cell temperature (Jakhrani et al., 2011).

S/n	Author(s)	Empirical models	Comments
1	Didier (2001)	$T_c = T_a + \frac{(T_c NOCT - 20)}{800}(219 + 832\frac{=}{Kt})$ $Cf = 1 - 1.17 \times 10^{-4} (S_m - S)^2$	For non-optimal values, use a multiplier with Sm denotes optimal tilt angle and S is the actual tilt angle (degrees)
2	Krauter (2004)	$T_C = T_a + KG_T$, and K = 0.0058, 0.012 and 0.03	The value of k for lower, upper and usual modules
3	Mondol et al., (2005 and 2007)	$T_C = T_a + 0.031G_T$, and $T_C + 0.031G_T - 0.058$	Tc is taken as mean of front and back temp. of module °C, Vw > 1 m/s with constant U_L
4	Duffie and Beckman (2006)	$T_c = T_a + \left[\left(\frac{G}{G_{NOCT}}\right)\left(\frac{U_{LNOCT}}{U_L}\right)(T_{CNOCT} - T_{aNOCT})\left(1 - \frac{n_c}{\tau_a}\right)\right]$	The value of transmittance and absorbance product ($\tau\alpha$) was taken as 0.9 Coefficient of heat losses (U_L) was associated
5	Chenni et al., (2007)	$T_C = 0.943T_a + 0.028G_T - 1.528V_W + 4.3$	Coefficient of heat losses (U_L) was not taken into account

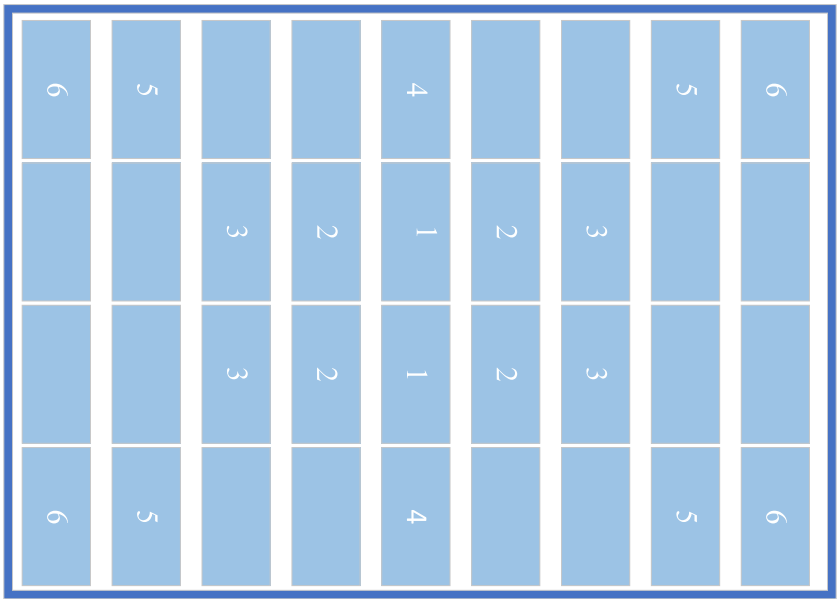

Fig. 3. Cell mapping on the 36 Cell 13 Wp PV Module.

In the cell mapping procedure, the cells in the same matrix are almost at the same distance from the centre-most cells and were assumed to be at the same temperature. One cell from each matrix designation cluster was randomly selected for actual measurements. Fig. 4(a) shows the front side of the cell matrix mapping. The temperature thermocouples (K-type) used to measure the individual cell temperatures were stuck on the Polyvinyl Fluoride (PVF) layer at the back side of the PV cells using industrial heat resistant tape as in Fig. 4(b). The thermocouples were then covered with another industrial adhesive to firmly bind them to the PVF back plate whose thermal conductivity (k) is 0.25 W/mK as per the manufacturer's specifications. This preliminary setup was fabricated to enable measurement of the individual bare cell temperatures before subsequent fabrication of systematic measurement setups. The module was mounted horizontally on a wooden structure, 1 metre above the ground and there was free circulation of air around and during the measurements. The wind speed was fairly low ranging between 0 and 0.3 metres per second. The setup was then subjected to solar radiation and the data logged using an 8-channel KEYENCE NR500 data logger. Temperature measurements from the 6 representative cells selected from the designated matrices are taken over a period of 125 min at intervals of 30 s and the logged data was thereafter transferred to a computer in CSV file format for analysis.

Table 2
Bare cell matrix temperature variance.

Matrix number	Variance (%)	Total variance (%)
Matrix 1 Th 1	−19.39 to 18.88	38.28
Matrix 2 Th 2	−23.39% to 15.2	38.59
Matrix 3 Th 3	−23.86 to 14.16	38.02
Matrix 4 Th 4	−23.06 to 15.12	38.18
Matrix 5 Th 5	−5.78 to 28.16	33.94
Matrix 6 Th 6	−7.4 to 25.44	32.84

3.3. Systematic solar PV cell temperature measurements setups under TIMs

After the preliminary cell mapping and bare cell temperature measurements setup, eight centre most cells of the 36 cells PV module were designated for systematic cell temperature measurements for further investigations. The eight cells were all drawn from the three central matrices mapped earlier and designated as Matrix 1, Matrix 2 and Matrix 3. Once again, a representative cell was randomly chosen for placement of the temperature measurement thermocouples. Three K-type thermocouples were stuck on the TIMs under the PVF back plate as shown in Fig. 5(a), (b) and (c). The three thermocouples are designated as Th 1, Th 2 and Th 3 and used to collect the cell temperature data when the

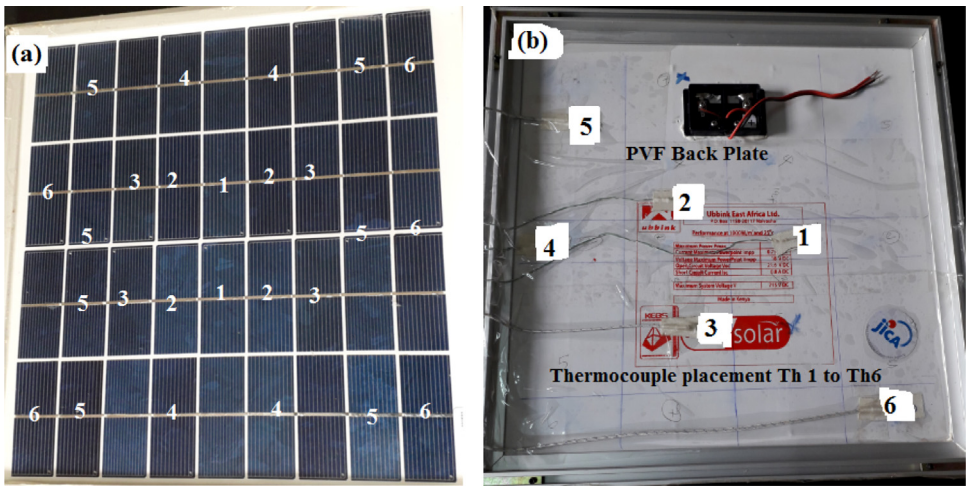

Fig. 4. Cell mapping for temperature distribution measurements; (a) PV cell mapping, (b) Thermocouple placement.

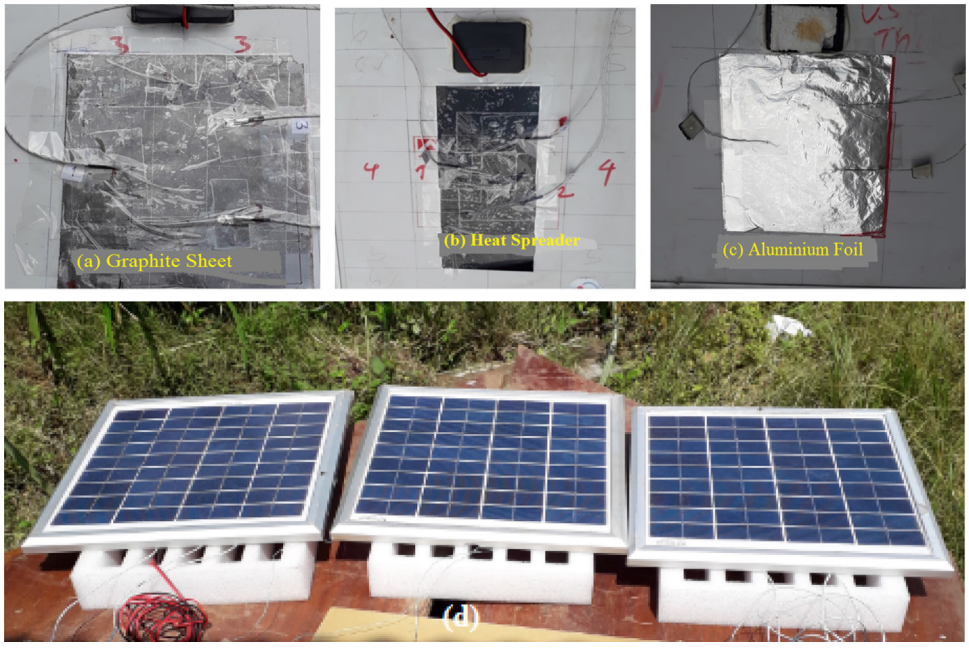

Fig. 5. Systematic temperature distribution measurements using various TIMs; (a) Graphite (b) Heat spreader (c) Aluminium foil (d) Complete setup of the three sets.

module is exposed to natural solar radiation as in Fig. 5(d). The three module setups were fabricated using graphite sheet TFO-S250-CB of 0.27 mm gauge thickness and a thermal conductivity (k) of 35 W/mK, PH-3 heat spreader (H.S) sheet with thermal conductivity (k) of 400 W/mK and gauge thickness of 0.30 mm and clean aluminium foil sheet of 0.32 mm gauge thickness and thermal conductivity (k) of 235 W/mK as in Fig. 5(a), (b) and (c), respectively.

This setup is fabricated to observe the effects of TIMs on cell temperature distribution on the three matrices, measured as Th 1, Th 2 and Th 3 and also to form a basis for the subsequent measurements. During the data analysis, the variance in temperature was evaluated as a percentage difference between the mean of the measured cell matrix temperatures and the individual cell matrix temperatures in each case.

3.4. PV-TEG temperature and voltage measurements under TIMs

In this subsection, four setups were fabricated where the four central cells of the PV module are designated for the measurement procedures. The three PV–TIM–TEG setups and a control setup (PV–TEG) were investigated under air- and water-cooled environments. Having looked at the effects of TIMs on the temperature distribution, this particular investigation was meant to bring out their actual significance on the PV–TEG power generation assembly. In studying the effects of temperature mismatch on TEG voltage output, two thermocouples and two TEGs were used to measure cell temperature and voltage output, respectively in each setup. These measurements were referenced to the centre-most Matrices 1 and 2 of the initial cell mapping as earlier shown in Fig. 3. The temperature and voltage measurements were first conducted under passive air cooling and later under passive water cooling where a honeycomb aluminium cooling panel was used as the heat sink. The cells on Matrix 1 and 2, are selected

Fig. 6. Air- and water-cooled PV–TIM–TEG setups 1 and 2 (a) graphite (b) heat spreader (c) aluminium foil (d) bare cells.

after confirmatory results from the previous measurements revealed uneven temperature distribution on the entire module. The three setups are fabricated using the three different TIMs sandwiched between the PV modules' PVF back plate and the TEG hot side and then thermocouples stuck on the TIMs at the edges of each TEG module space to measure the PV cells temperature. The fourth module used as the reference had its thermocouples stuck on the PVF cell matrix leaving space where the TEGs were to rest. Before the thermal interface materials were applied on the PV back sheet, the PVF was well cleaned using a solvent cleaner fluid to remove all particles and any oily dust on the surface. The TIMs were then each laid flat on the PVF avoiding any air being trapped in between. An industrial adhesive was then used to firmly hold the TIM on the PVF. The TEG modules were stuck on the honeycomb cooling panel from their cold side so that they rest square on the TIMs and PVF where the complete assemblies were mechanically clamped together at same safe mechanical loading of 4.8 kPa that is within the safe standard loading of 5.4 kPa for PV cells. The four setup assemblies are then mounted outdoors horizontally under both air and water cooling as in Fig. 6 and then exposed to solar radiation. Fig. 6 setup 1 (a) (b) (c) and (d), represent the Aluminium foil, Heat spreader, graphite sheet and bare cell modules, respectively while Fig. 6 setup 2 similarly shows the same configuration under water cooled conditions.

Water cooling was used to study its significance on temperature distribution and TEG voltage patterns because water has a higher heat capacity, density, thermal conductivity and would be preferred when available especially where water is easily accessible (Yin et al., 2017). These water-cooled setups would also inform the proposed actual design of the PV–TEG system for a Recirculation Aquaculture System (RAS) at a lakeside site in Nyalenda Kisumu, Kenya as previously reported in our study (Guyo et al., 2020). The TEG voltage output and the PV cell temperatures are once again simultaneously logged using a KEYENCE NR500 data logger.

During this setup, the primary aspects under study are the temperature distribution across each module, notably mismatch under the PV cells and how the mismatch affected the voltage generated by the TEG modules below the PV cells.

4. Results and discussions

The discussion of our findings is split into three main parts. First, we report the variation characteristics of temperature mismatch between the PV cells of the same module and compare the measured cell temperature variances, the second part examines the results obtained when the thermal interface materials are used under the PV module to improve the temperature distribution. Lastly, we report on the effects of using the three thermal interface materials, on the temperature and TEG voltage output mismatch.

4.1. Analytical solution and preliminary PV bare cell temperature measurements

The PV cell temperature analytic solution sought to provide an assessment of the cell temperature under the conditions and environment of measurement. These results provided the representative module cell temperature for the 36 cells on the PV module. This cell temperature was then be used as the normalized reference cell temperature for comparison with the measured cell temperatures under those conditions and environment. The analysis results are presented in Fig. 7(a) showing how the cell temperature varied with irradiation, ambient temperature, and the mean of the measured cell matrix temperatures. The graph of the mean of the measured cell matrix temperatures closely traces the analytic temperature curve validating the entire process. The slight difference observed of between −9.3% and 8.66% with an average of 1.97% between the measured mean and simulated temperature accounts for the temperature variance between the individual cell matrices. Both the temperatures were responsive to the amount of irradiance available and responded sluggishly to the ambient temperature as in Fig. 7(a). During this experiment, the irradiance varied between 160 W/m^2 and 960 W/m^2 and the

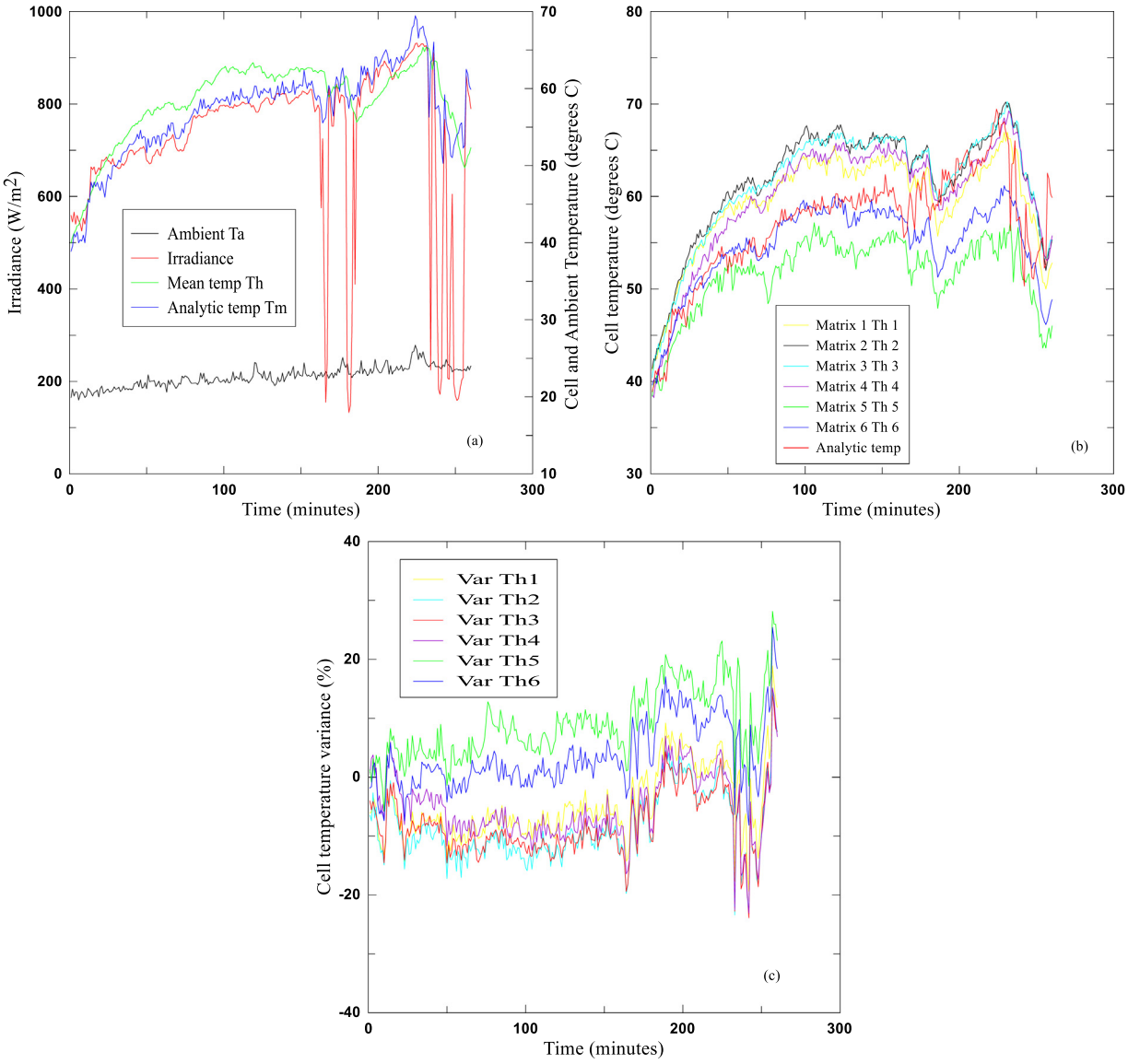

Fig. 7. (a) Irradiance & temperatures, (b) Measured & analytic temperature (c) Matrix temperature variance.

ambient temperature varied between 19.9 °C and 26.7 °C and resulted in the analytically evaluated PV cell temperatures that varied between 30.82 °C and 69.84 °C.

From the temperature measurement results, it is observed that the measured cell temperatures are indeed different as shown in Fig. 7(b) as opposed to the general expectation that they would be the same since the cells are exposed to uniform irradiance (Soliman et al., 2019; Li et al., 2019). These measured cell temperature results also confirm and agree with the findings by Tina and Abate (2008) who observed higher cell temperature at the most central cell compared with the outer cells. In Fig. 7(b), the simulated cell temperature is too plotted to compare it with the measured temperatures and the graph fits closely among the measured matrix cell temperature response plots. Fig. 7(c) then shows the variance of the measured individual cell matrix temperatures as compared to the simulated temperature and Table 2 further presents the summary of variance for each cell matrix.

As observed in Table 2, there is high temperature variance between the cell matrix temperatures and the analysed cell temperature with variances ranging from 32.84% on matrix 6 to a high of 38.59% on matrix 2. This cell matrix temperature variance is expected to create a corresponding variance in the operating temperature gradient ΔT of the TEG modules that are coupled to the PV cells making them generate voltages at different MPPs (Montecucco et al., 2014) due to their varying hot side temperatures, *Th* as in Eq. (1). When the generated voltages and currents are different, series strings and parallel interconnections of TEG modules results in voltage conflicts and current mismatches that lead to power losses just like in PV and battery systems. In principle, the higher potential TEG string shall drive current towards the lower potential string until the two voltages become equal (Royne et al., 2005). Based on this observation, it is therefore beneficial to make the cell temperatures at the hot side of the TEG modules as uniform as possible. This would ensure the TEG modules generate uniform or near uniform voltage resulting in reduced or no interconnection power losses (Zhang et al., 2020a).

4.2. Systematic PV cell temperature distribution measurements under TIMs

In this sub-section, the temperature responses of three thermal interface materials are examined graphically following the

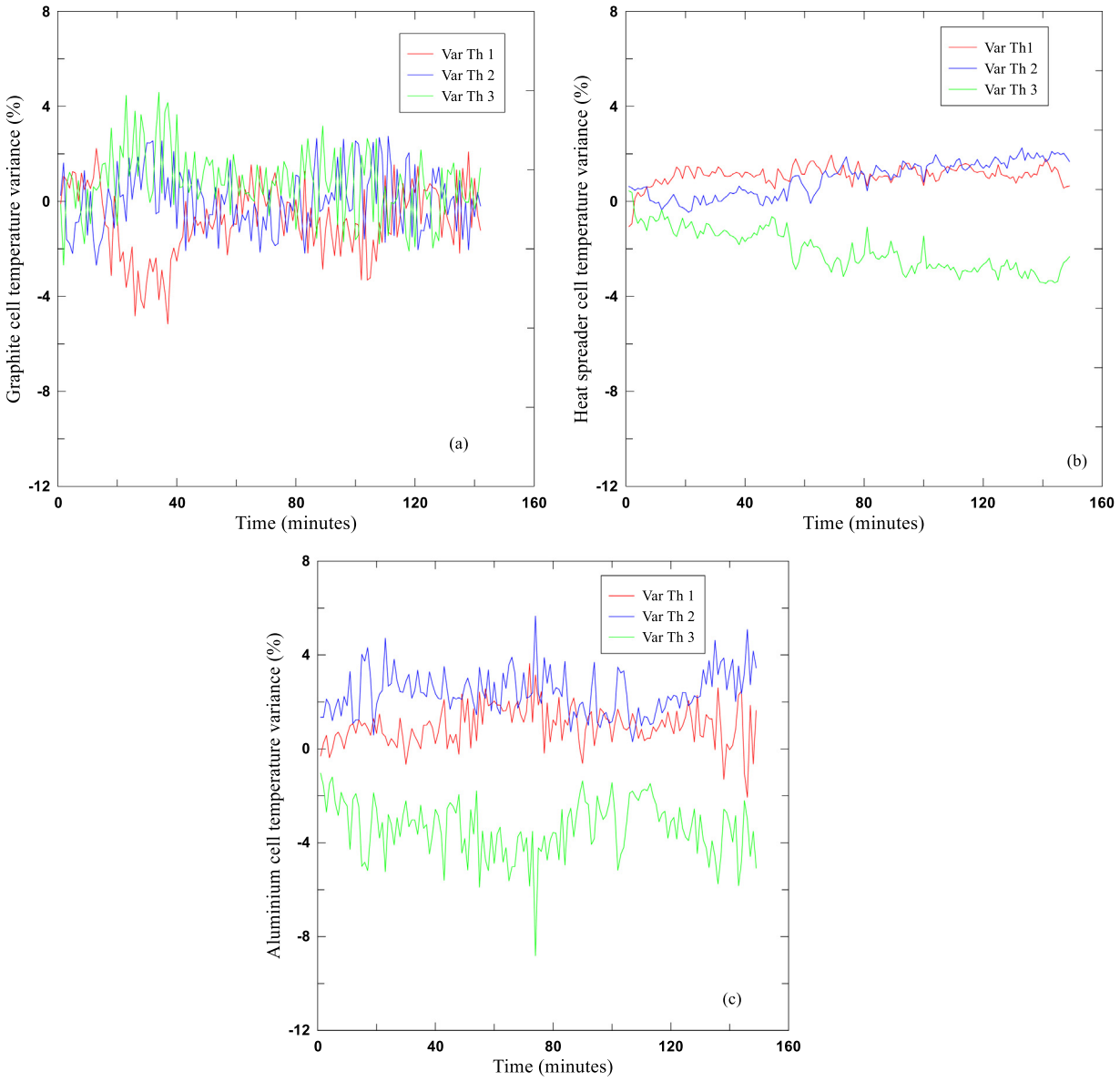

Fig. 8. Variance on PV cell temperature distribution under different TIMs (a) graphite sheet (b) heat-spreader (c) aluminium foil.

observations made from temperature variance between the bare PV cells in the preceding setups. Fig. 8 shows the temperature response of the PV cells under the TIMs with the modules being subjected to the same irradiance. The mean of the measured cell matrix temperatures from each module, is used to determine the percentage temperature variance of each cell matrix. Results obtained from this experiment show the cells under graphite TIM having a temperature variance ranging between −5.17% and 4.59% which translates to 9.76% and graphically presented in Fig. 8(a). The heat spreader has a variance ranging between −3.45% and 2.25% which yields a 5.7% variance overall {Fig. 8(b)} and the aluminium foil has a variance ranging between −8.81% and 6.41% which is 15.22% as also presented graphically in Fig. 8(c). The variances observed under the TIMs are way below what was observed when the temperatures were measured on bare cells where the variance was ranging between 32.84% and 38.59% that were also measured under normal open air cooling conditions. This translated to PV cell temperature mismatch mitigation of 70.3%–74.7%, 82.6%–88.2% and 53.7%–60.6% for the three TIMs; graphite, HS and aluminium foil, respectively.

It is observed that among the TIMs used, the heat spreader presented the lowest cell temperature variance followed by the graphite sheet and the aluminium foil presented the highest variance. The thermal conductivity of the TIMs contributed a lot to the observed temperature variance though the aluminium TIM did not behave as was expected. The divergent performance of the aluminium TIM could have been attributed to surface texture and presence of micro-scale roughness (Chen and Xuan, 2015) and probably the difference in the Coefficient of Thermal Expansion (CTE) of the three materials where say, for aluminium, α is $(21–24)\times10^{-6}/°C$ and $(4–8)\times10^{-6}/°C$ for graphite (Chen and Huang, 2013). With the reduced cell temperature variance by the TIMs, it is expected that the temperature distribution on the TEG modules shall subsequently be uniform and/or almost equal. This temperature uniformity is also expected to create a uniform ΔT across the TEG modules that will generate uniform voltages.

4.3. PV cell temperature and TEG voltage measurements under tims

In this sub-section, the effects of module temperature on TEG voltage generation under three thermal interface materials are

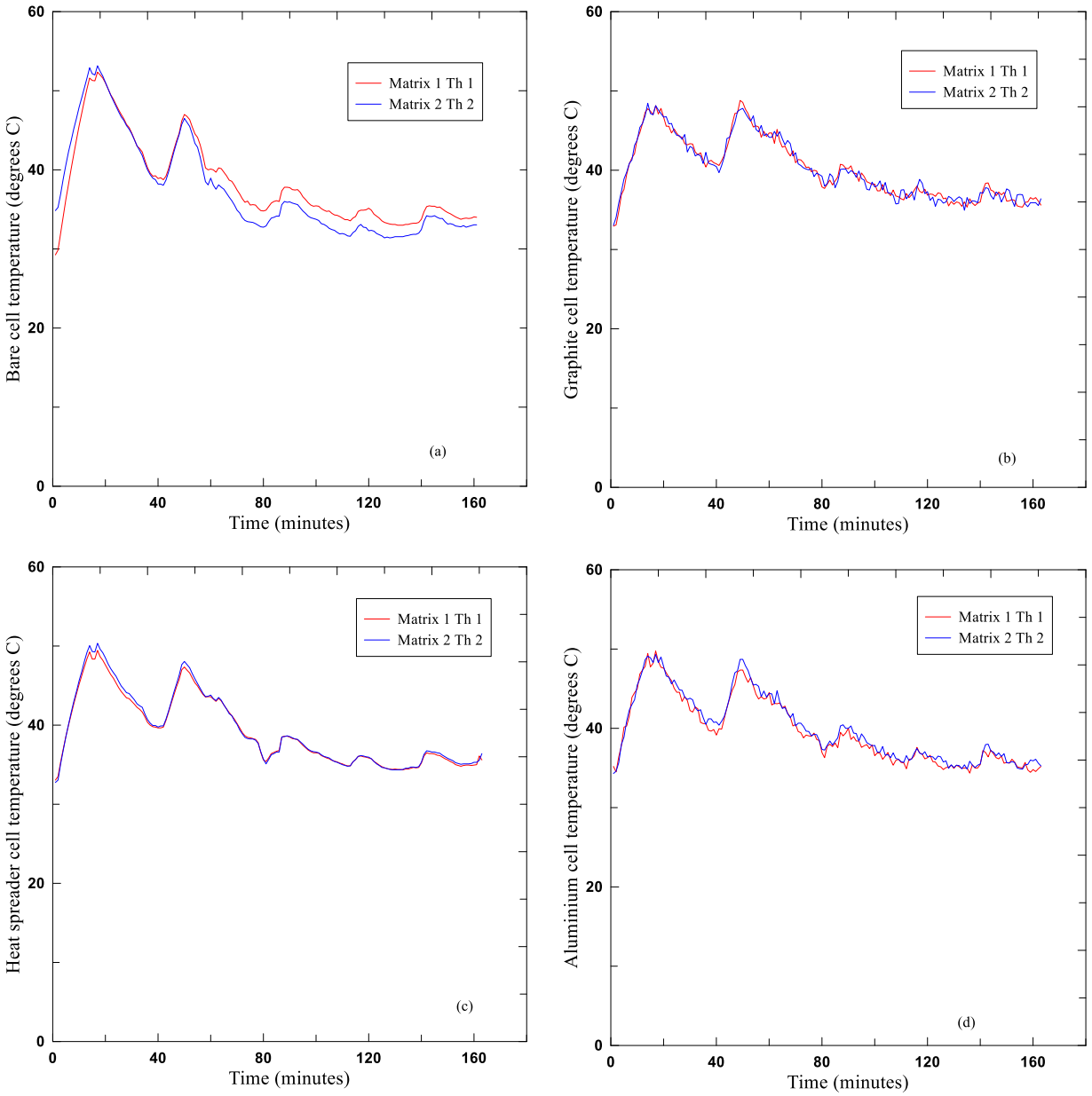

Fig. 9. PV–TEG cell temperature distribution behaviour with time under air-cooled environments (a) bare cell (b) graphite sheet (c) heat spreader (d) aluminium foil.

examined experimentally following the observations made in the preceding setups where the TIMs improved the temperature distribution at the back of the PV cells.

4.3.1. PV-TIM-TEG under air cooled environments

In these setups, the variance in both temperature and voltages is calculated as a percentage difference of the actual measured values to the mean of the measured values. During this experiment, the sky was partially clear with some cloud casts and fluctuating irradiance that started at 990 W/m^2 then briefly dropped to 466 W/m^2 and later rose to a peak of 988 W/m^2. By the end of the measurements period, irradiance had reduced to 287 W/m^2 maintaining an average irradiance of 735.3 W/m^2.

The bare cells setup presented the highest temperature and voltage variance, at ±8.7% for temperature and ±28.64% for voltage as shown in Fig. 9(a) and 10 (a), respectively due to the setup intervention conditions and dominant weather as compared with the open air conditions in Section 4.1. The heat spreader setup on the other hand, presented the lowest temperature variance at ± 0.98% and a voltage variance of ±1.71% as shown in Fig. 9(c) and 10 (c), respectively. The graphite sheet setup presented temperature variance of ±2.19% and a voltage variance of ±5.49% as shown in Figs. 9(b) and 10(b), respectively. Finally, the aluminium foil setup presented temperature variance of ±2.31% and a voltage variance of ±7.83% as shown in Figs. 9(d) and 10(d), respectively.

The results in Figs. 9 and 10 confirm that temperature mismatch reduced significantly when thermal interface materials are used. The temperature mismatch for the TIM modules was much lower with the lowest being a total variance of 1.96% with the heat spreader. This low variance when using the TIMs resulted into a maximum TEG voltage variance of 3.42% compared with that of the bare cells of 56.8%. The observed high voltage variance in the bare cell TEGs is due to the micro scale roughness of the PVF and the ceramic surface of the TEGs (Chen and Xuan, 2015; Zhang and Zhao, 2015; Zhang et al., 2020b). Once again the aluminium foil presented higher variances than the graphite sheet for reasons cited earlier on surface texture and CTE, but still

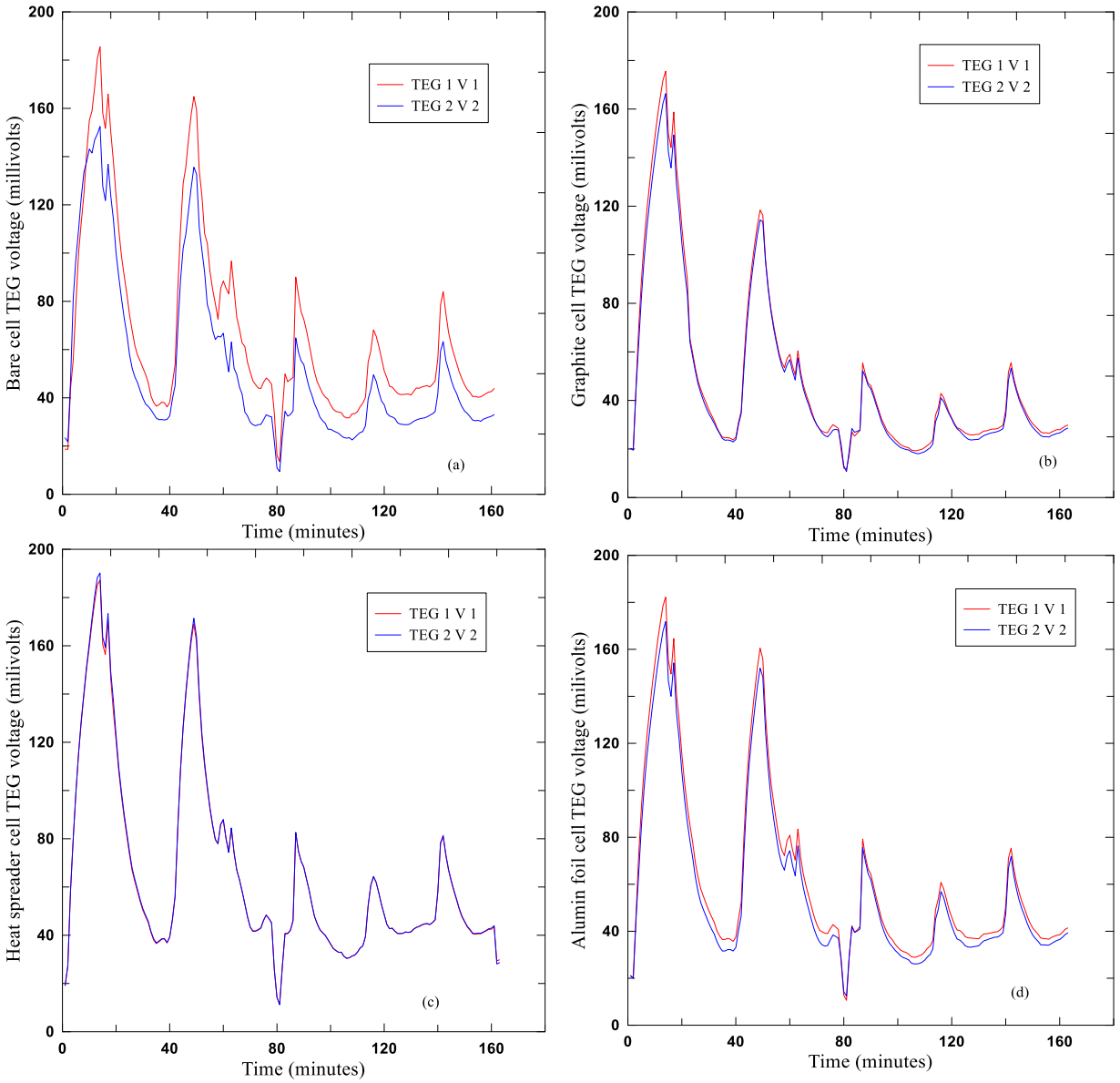

Fig. 10. TEG voltages under air cooled TIMs (a) bare cell (b) graphite (c) heat spreader (d) aluminium foil.

far better than the bare cell variances (Chen and Xuan, 2015; Chen and Huang, 2013).

The results obtained in this setup are a clear disclosure that when PV–TEG hybrid systems are well coupled using the right TIM with the lowest Thermal Contact Resistance (TCR), the performance of the TEG voltage output is significantly improved (Zhang et al., 2020b; Li et al., 2014; Lin et al., 2015).

4.3.2. PV-TIM-TEG under water cooled environments

Similarly, in this measurement, the variance in both temperature and voltages is calculated as a percentage difference of the actual measured values to the mean of the measured values. During these measurements, the temperature of the cooling water rose from 22.8 °C at the start to 24.7 °C by the end of measurements. The sky was very clear most of the time and the average irradiance was generally above 860 W/m^2 starting from 868 W/m^2 and rising to a high of 905 W/m^2 and later rising above 936 W/m^2. Once again in this setup, the bare cells setup had the highest temperature and voltage variance at ±5.58% and ±19.77%, respectively as shown in Figures 11 (a) and 12 (a). The heat spreader once again exhibited the lowest temperature variance at ±0.82% and a voltage variance of ±1.62% as shown in Figs. 11(c) and 12(c). While the graphite sheet presented temperature variance of ±1.96% and a voltage variance of ±2.86% as shown in Figs. 11(b) and 12(b). Here also the aluminium foil presented higher temperature variance of ±2.17% and a voltage variance of ±3.18% as shown in Figs. 11(d) and 12(d) despite the fact that aluminium has a higher thermal conductivity than the graphite sheet. This performance is attributable to reasons cited earlier on surface texture and effects of CTE in section 4.3.1 (Chen and Xuan, 2015; Chen and Huang, 2013).

Results obtained in 4.3.1 and 4.3.2 show that temperature mismatch results in a proportional mismatch on TEG voltage output such that as the mismatch increases, the voltage difference also increases. Figs. 9(a), 10(a), 11(a) and 12(a) reveal the usual effect of the temperature gradient, ΔT in PV–TEG systems on the TEG voltage output as reported in ÖZBAŞ (2019). The cooling water temperature maintained a higher ΔT that resulted in higher voltage output in the water cooling as compared in the air cooling setups and this confirms that water has better cooling properties (Zhang et al., 2020a). In the water-cooled setup, the highest or peak total TEG voltage was 604.14 mV generated under

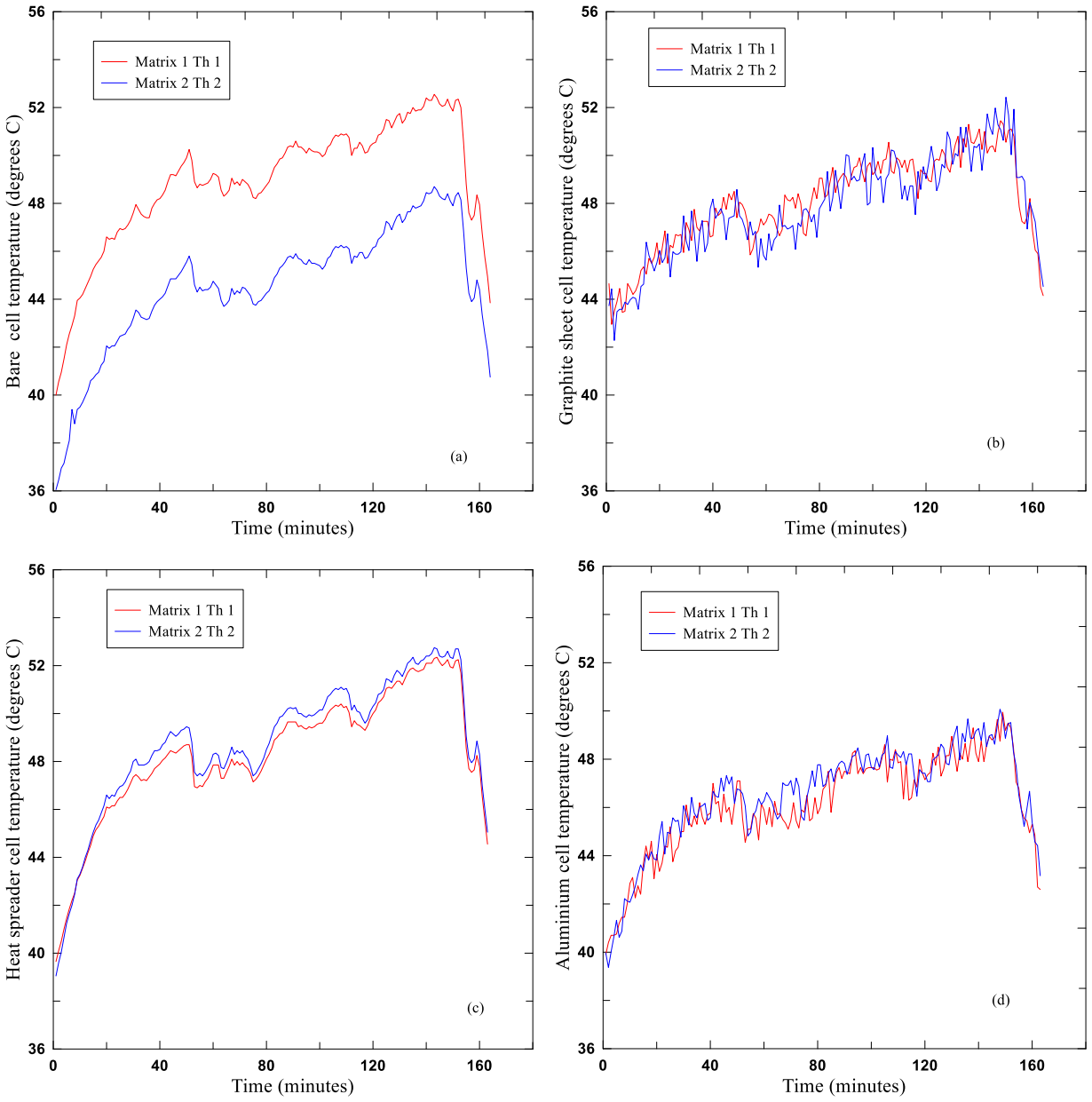

Fig. 11. Cell temperature distribution behaviour with time under water-cooled environment (a) bare cell (b) graphite (c) heat spreader (d) aluminium foil.

the heat spreader as compared to a high of 377.4 mV for the air-cooled setup generated under the same TIM.

With the PV module physical dimensions (L×W× H) as 325 mm × 325 mm × 20 mm and those of the TEG module (L×W×H) being 40 mm × 40 mm ×3.4 mm and while accounting 25% dead space between TEGs and PV edges, the PV module would comfortably accommodate 49 TEG modules on its back plate. From the best results obtained under air cooling with TIM (H.S), the total TEG voltage for each PV–TEG assembly shall be 9.31 V (Voc) at an irradiance of 972 W/m^2 and a temperature of 50.05 °C, while the PV module alone generates about 19.41 V (Voc) under the same conditions, calculated using the manufacturer's Temperature Coefficient of Voltage (TCV) of −0.0875 V/°C. The water cooled system under the same TIM (H.S) on the other hand would yield a TEG voltage of 15.03 V (Voc) at an irradiance of 905 W/m^2 and temperature of 49.05 °C, while the PV module generates about 19.5 V (Voc) under the same conditions. Therefore, an additional 47.96% voltage is realized from the TEG system when HS is used under air cooling and an additional 77.08% voltage under water cooling.

Without any mode of cooling, at irradiance of 933 W/m^2 the PV bare cells temperature rose to 63.32 °C and the ambient temperature was 26.1 °C, while at an irradiance of 908 W/m^2 the cell temperature corresponded to 62.62 °C and the ambient temperature was around 23.65 °C, from the results obtained in Section 4.1. Using a TCV of −0.0875 V/°C, the PV (Voc) is calculated to be 18.25 V (Voc) at 63.32 °C and 18.31 V (Voc) at a cell temperature of 62.62 °C. So, the voltage gain on air cooling under HS at irradiance of 933 W/m^2 at a cell temperature of 44.65 °C as in Section 4.3.1, is 8.93%. While the voltage gain under water cooling on HS at irradiance of 907 W/m^2 at a cell temperature of 48.8 °C, is 6.96%. On average both the methods of cooling save above 5% of the bare cell PV open circuit voltage.

The three investigated TIMs offered relatively similar improvements in temperature distribution under the PV that resulted in voltage gain compared with the bare cell PV. The main factor that affected the performance of the TIMs was their texture, surface

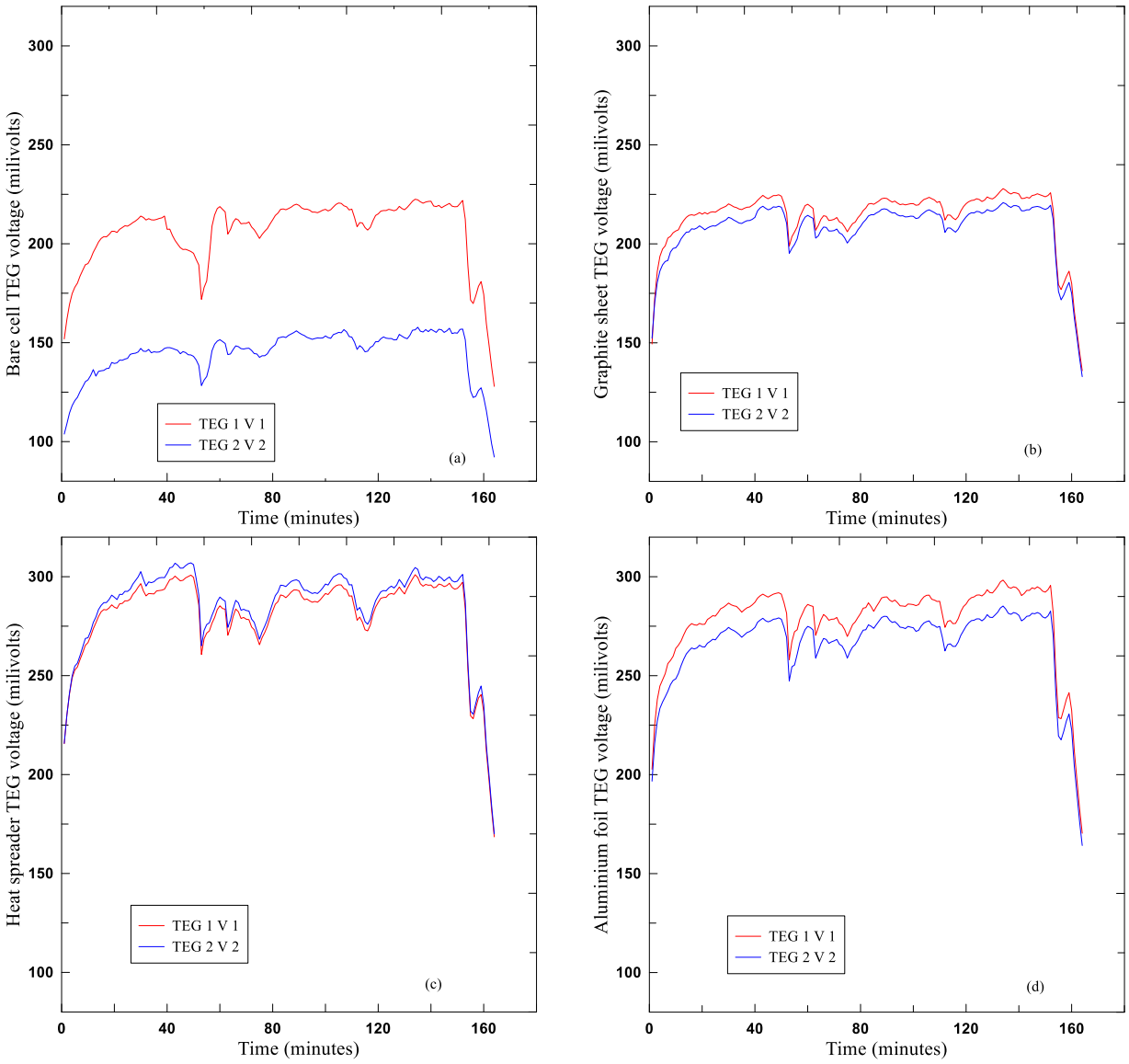

Fig. 12. TEG voltages under water cooled TIMs (a) bare cell (b) graphite (c) heat spreader (d) aluminium foil.

roughness and the thermal conductivity as observed by Li et al. (2014) the performance of the graphite sheet and aluminium foil could probably improve if some silica-gel (with tolerance of 200 °C) is used on the surface to reduce the air trapped between the surfaces (Li et al., 2014)

Overall, the PV–TIM–TEG system realized an additional power gain of 1.8% and 2.5% from the PV module under air and water cooling, respectively, when HS TIM is used compared with a no cooling scenario. The total additional power improvements from the PV–TIM–TEG assembly under water-cooled environment is 24.85% based on the best output, while with air cooling, a gain of 19.7% at best output was realized.

5. Conclusions

Investigations on temperature mismatch show that bare cells have higher temperature variance of ±8.7% with a corresponding higher voltage variance of ±28.64% under air cooling and temperature variance of ±5.58% and a voltage variance of ±19.77% under water cooling. Use of TIMs significantly mediates PV cell temperature variance resulting in remarkable TEG voltage output improvements in the PV–TIM–TEG system setup. Furthermore the efficient heat transfer also results in considerable reduction of the PV cell temperature improving its voltage and power output. For the three investigated TIMs, the heat spreader, PH-3, showed the lowest temperature and voltage variance under both air and water-cooled conditions. The effect of using TIMs (HS) in cooling the PV cells resulted in additional power of 19.7% under air cooling and 24.85% when water-cooled with the benefits increasing at higher temperatures. Hence remarkable results have been realized in this study with a sum total gain of 21.5% with air cooling and 27.35% with water cooling when heat spreader is used, which gives an opportunity to investigate other emerging TIMs.

Abbreviations

CSV	Comma Separated Values
CTE	Coefficient of Thermal Expansion
ΔT	Temperature Gradient
G	Total Irradiance in W/m^2
H	Height
HS	Heat spreader
I_{sc}	Short Circuit Current

IV	Current Voltage
K	Thermal Conductivity
kPa	Kilo Pascal's
MPP	Maximum Power Point
mV	milli Volts
NOCT	Nominal Operating Cell Temperature
PV	Photovoltaic
P_{TEG}	Thermoelectric Generator Power
S	Cross Sectional Area
PVF	Polyvinyl Fluoride
RAS	Recirculation Aquaculture System
R_e	Reynolds Number
R_L	Load Resistance
R_{TEG}	TEG Internal Resistance
T_a	Ambient Temperature in °C
T_{mod}	Module Temperature
T_C	PV Cell Temperature in °C
T_{aNOCT}	Ambient Temperature According to SRE set at 20 °C
T_{cNOCT}	Cell Nominal Operating Temperature
G_{NOCT}	Total Solar Irradiance at NOCT according to SRE set at 800 W/m^2
TCV	Temperature Coefficient of Voltage
TEG	Thermoelectric Generator
TEM	Thermoelectric Material
T_c	Cold side Temperature
T_h	Hot side Temperature
TIM	Thermal Interface Material
TCR	Thermal Contact Resistance
VicInAqua	Victoria Integrated Aquaculture
Voc	Open Circuit Voltage
V_w	Wind Speed in m/s
Wp	Watts Peak
Wt.	Water
Zt	Figure of Merit

Greek Symbols

α	Seebeck Coefficient (V/K)
τ_α	Product to Transmittance–Absorption Estimated at 0.9
η_C	Conversion Efficiency of PV Cell from Manufactures Data sheet

CRediT authorship contribution statement

Gideon Kidegho: Conceptualization, Methodology, Investigation Preliminary data analysis, Writing the revised draft. **Francis Njoka:** Data curation, Formal analysis, Visualization, Review and editing of the revised draft. **Christopher Muriithi:** Review and editing revised draft, Supervision. **Robert Kinyua:** Resources, Funding acquisition, Supervision, Project administration.

Declaration of competing interest

The authors declare that they have no known competing financial interests or personal relationships that could have appeared to influence the work reported in this paper.

Acknowledgments

This work is supported by the European Union's Horizon 2020 research and innovation programme under grant agreement No. 689427 through the 'VicInAqua' project.

References

Abu-Rahmeh, T.M., 2017. Efficiency of photovoltaic modules using different cooling methods: A comparative study. J. Power Energy Eng. 05, 32–45. http://dx.doi.org/10.4236/jpee.2017.59003.

Atsu, D., Dhaundiyal, A., 2019. Effect of ambient parameters on the temperature distribution of photovoltaic (PV) modules. Resources 8, 107. http://dx.doi.org/10.3390/resources8020107.

Bahaidarah, H.M.S., Baloch, A.A.B., Gandhidasan, P., 2016. Uniform cooling of photovoltaic panels: A review. Renew. Sustain. Energy Rev. 57, 1520–1544. http://dx.doi.org/10.1016/j.rser.2015.12.064.

Belkaid, A., Colak, I., Kayisli, K., Bayindir, R., Bulbul, H.I., 2018. Maximum power extraction from a photovoltaic panel and a thermoelectric generator constituting a hybrid electrical generation system, içinde. In: 2018 International Conference on Smart Grid (IcSmartGrid). IEEE, Nagasaki, Japan, pp. 276–282. http://dx.doi.org/10.1109/ISGWCP.2018.8634534.

Chandrasekar, M., Senthilkumar, T., 2015. Experimental demonstration of enhanced solar energy utilization in flat PV (photovoltaic) modules cooled by heat spreaders in conjunction with cotton wick structures. Energy 90, 1401–1410. http://dx.doi.org/10.1016/j.energy.2015.06.074.

Chen, J.K., Huang, I.S., 2013. Thermal properties of aluminum–graphite composites by powder metallurgy. Composites B 44, 698–703. http://dx.doi.org/10.1016/j.compositesb.2012.01.083.

Chen, Y., Xuan, Y., 2015. The influence of surface roughness on nanoscale radiative heat flux between two objects. J. Quant. Spectrosc. Radiat. Transfer. 158, 52–60. http://dx.doi.org/10.1016/j.jqsrt.2015.01.006.

Creutzig, F., Agoston, P., Goldschmidt, J.C., Luderer, G., Nemet, G., Pietzcker, R.C., 2017. The underestimated potential of solar energy to mitigate climate change. Nat. Energy 2, 17140. http://dx.doi.org/10.1038/nenergy.2017.140.

Dalala, Z., Saadeh, O., Bdour, M., Zahid, Z., 2018. A new maximum power point tracking (MPPT) algorithm for thermoelectric generators with reduced voltage sensors count control †. Energies 11, 1826. http://dx.doi.org/10.3390/en11071826.

Deng, Y., Zhu, W., Wang, Y., Shi, Y., 2013. Enhanced performance of solar-driven photovoltaic–thermoelectric hybrid system in an integrated design. Sol. Energy 88, 182–191. http://dx.doi.org/10.1016/j.solener.2012.12.002.

Dousti, M.J., Petraglia, A., Pedram, M., 2015. Accurate electrothermal modeling of thermoelectric generators, içinde. In: Design, Automation & Test in Europe Conference & Exhibition (DATE), 2015. IEEE Conference Publications, Grenoble, France, pp. 1603–1606. http://dx.doi.org/10.7873/DATE.2015.0516.

Duffie, J.A., Beckman, W.A., 2013. Solar Engineering of Thermal Processes: Duffie/Solar Engineering 4e. John Wiley & Sons, Inc., Hoboken, NJ, USA, http://dx.doi.org/10.1002/9781118671603.

Ferrara, C., Philipp, D., 2012. Why do PV modules fail?. Energy Procedia 15, 379–387. http://dx.doi.org/10.1016/j.egypro.2012.02.046.

Fisac, M., Villasevil, F.X., López, A.M., 2014. High-efficiency photovoltaic technology including thermoelectric generation. J. Power Sources 252, 264–269. http://dx.doi.org/10.1016/j.jpowsour.2013.11.121.

Geisz, J.F., France, R.M., Schulte, K.L., Steiner, M.A., Norman, A.G., Guthrey, H.L., Young, M.R., Song, T., Moriarty, T., 2020. Six-junction III–V solar cells with 47.1% conversion efficiency under 143 Suns concentration. Nat. Energy 5, 326–335. http://dx.doi.org/10.1038/s41560-020-0598-5.

Guyo, Kidegho G., Robert, Kinyua., Christopher, Muriithi., Francis, Njoka., 2020. Innovative solar photovoltaic and thermoelectric power generator for a recirculating aquaculture system. Int. J. Renew. Energy Res. IJRER 10 (3), (2020).

Huld, T., Amillo, A., 2015. Estimating PV module performance over large geographical regions: The role of irradiance, air temperature, wind speed and solar spectrum. Energies 8, 5159–5181. http://dx.doi.org/10.3390/en8065159.

Jakhrani, A.Q., Othman, A.K., Rigit, R.A.H., Samo, S.R., 2011. Comparison of solar photovoltaic module temperature models. World Appl. Sci. J. (Special Issue of Food and Environment) 14.

Kasim, N.K., Hussain, Hazim H., Abed, Alaa N., 2019. Performance analysis of grid-connected CIGS PV solar system and comparison with PVsyst simulation program. Int. j. smart grid. 3, 172–179.

Kishore, R.A., Sanghadasa, M., Priya, S., 2017. Optimization of segmented thermoelectric generator using Taguchi and ANOVA techniques. Sci. Rep. 7, 16746. http://dx.doi.org/10.1038/s41598-017-16372-8.

Li, K., Liu, C., Chen, P., 2014. A 1 KW thermoelectric generator for low-temperature geothermal resources, içinde. In: Thirty-Ninth Workshop on Geothermal Reservoir Engineering. Stanford University, Stanford, California, p. 12.

Li, Y.-R., Su, C.-C., Chang, S.-H., 2019. Applying aluminum–vertically-aligned carbon nanotube forests composites for heat dissipation. Nanomaterials 9, 758. http://dx.doi.org/10.3390/nano9050758.

Lin, J., Liao, T., Lin, B., 2015. Performance analysis and load matching of a photovoltaic–thermoelectric hybrid system. Energy Convers. Manage. 105, 891–899. http://dx.doi.org/10.1016/j.enconman.2015.08.054.

Maturi, L., Belluardo, G., Moser, D., Del Buono, M., 2014. Bipv system performance and efficiency drops: Overview on PV module temperature conditions of different module types. Energy Procedia. 48, 1311–1319. http://dx.doi.org/10.1016/j.egypro.2014.02.148.

Montecucco, A., Siviter, J., Knox, A.R., 2014. The effect of temperature mismatch on thermoelectric generators electrically connected in series and parallel. Appl. Energy 123, 47–54. http://dx.doi.org/10.1016/j.apenergy.2014.02.030.

Nagayoshi, H., Kajikawa, T., 2006. Mismatch Power Loss Reduction on Thermoelectric Generator Systems Using Maximum Power Point Trackers, In: International Conference on Thermoelectrics.

ÖZBAŞ, Engin., 2019. Experimental investigation of passive water cooling in solar heating thermoelectric generator. J. polytechnic. http://dergipark.gov.tr/politeknik.

Paraskevas, A., Koutroulis, E., 2016. A simple maximum power point tracker for thermoelectric generators. Energy Convers. Manage. 108, 355–365. http://dx.doi.org/10.1016/j.enconman.2015.11.027.

Peng, Z., Herfatmanesh, M.R., Liu, Y., 2017. Cooled solar PV panels for output energy efficiency optimisation. Energy Convers. Manage. 150, 949–955. http://dx.doi.org/10.1016/j.enconman.2017.07.007.

R., Kiflemariam., M., Almas., Lin, C., 2014. Modeling Integrated Thermoelectric Generator-Photovoltaic Thermal (TEG-PVT) System, In: 2014 COMSOL Conference.

Rajkumar, V.A., Weijers, C., Debije, M.G., 2015. Distribution of absorbed heat in luminescent solar concentrator lightguides and effect on temperatures of mounted photovoltaic cells. Renew. Energy 80, 308–315. http://dx.doi.org/10.1016/j.renene.2015.02.003.

Royne, A., Dey, C., Mills, D., 2005. Cooling of photovoltaic cells under concentrated illumination: a critical review. Sol. Energy Mater. Sol. Cells 86, 451–483. http://dx.doi.org/10.1016/j.solmat.2004.09.003.

Sargunanathan, S., Elango, A., Mohideen, S.T., 2016. Performance enhancement of solar photovoltaic cells using effective cooling methods: A review. Renew. Sustain. Energy Rev. 64, 382–393. http://dx.doi.org/10.1016/j.rser.2016.06.024.

van Sark, W.G.J.H.M., 2011. Feasibility of photovoltaic – Thermoelectric hybrid modules. Appl. Energy 88, 2785–2790. http://dx.doi.org/10.1016/j.apenergy.2011.02.008.

Soliman, A.M.A., Hassan, H., Ahmed, M., Ookawara, S., 2020. A 3d model of the effect of using heat spreader on the performance of photovoltaic panel (PV). Math. Comput. Simul. 167, 78–91. http://dx.doi.org/10.1016/j.matcom.2018.05.011.

Soliman, A.M.A., Hassan, H., size, Effect.of.heat.spreader., 2019. Effect of heat spreader size microchannel configuration and nanoparticles on the performance of PV-heat spreader-microchannels system. Sol. Energy 182, 286–297. http://dx.doi.org/10.1016/j.solener.2019.02.059.

Soltani, S., Kasaeian, A., Sarrafha, H., Wen, D., 2017. An experimental investigation of a hybrid photovoltaic/thermoelectric system with nanofluid application. Sol. Energy 155, 1033–1043. http://dx.doi.org/10.1016/j.solener.2017.06.069.

Tang, Z.B., Deng, Y.D., Su, C.Q., Shuai, W.W., Xie, C.J., 2015. A research on thermoelectric generator's electrical performance under temperature mismatch conditions for automotive waste heat recovery system. Case Stud. Therm. Eng. 5, 143–150. http://dx.doi.org/10.1016/j.csite.2015.03.006.

Temaneh-Nyah, C., Mukwekwe, L., 2015. An investigation on the effect of operating temperature on power output of the photovoltaic system at university of namibia faculty of engineering and I.T campus, içinde. In: 2015 Third International Conference on Digital Information, Networking, and Wireless Communications (DINWC). IEEE, Moscow, Russia, pp. 22–29. http://dx.doi.org/10.1109/DINWC.2015.7054211.

Teo, H.G., Lee, P.S., Hawlader, M.N.A., 2012. An active cooling system for photovoltaic modules. Appl. Energy 90, 309–315. http://dx.doi.org/10.1016/j.apenergy.2011.01.017.

Tina, G.M., Abate, R., 2008. Experimental verification of thermal behaviour of photovoltaic modules, içinde. In: MELECON 2008 - the 14th IEEE Mediterranean Electrotechnical Conference. IEEE, Ajaccio, France, pp. 579–584. http://dx.doi.org/10.1109/MELCON.2008.4618497.

Yang, R.L., Tiepolo, G.M., Tonolo, É.A., Urbanetz Junior, J., de Souza, M.B., 2019. Photovoltaic cell temperature estimation for a grid-connect photovoltaic systems in curitiba. Braz. Arch. Biol. Technol. 62, e19190016. http://dx.doi.org/10.1590/1678-4324-smart-2019190016.

Yin, E., Li, Q., Xuan, Y., 2017. Thermal resistance analysis and optimization of photovoltaic-thermoelectric hybrid system. Energy Convers. Manage. 143, 188–202. http://dx.doi.org/10.1016/j.enconman.2017.04.004.

Zhang, J., Zhai, H., Wu, Z., Wang, Y., Xie, H., Zhang, M., 2020a. Enhanced performance of photovoltaic–thermoelectric coupling devices with thermal interface materials. Energy Rep. 6, 116–122. http://dx.doi.org/10.1016/j.egyr.2019.12.001.

Zhang, J., Zhai, H., Wu, Z., Wang, Y., Xie, H., Zhang, M., 2020b. Enhanced performance of photovoltaic–thermoelectric coupling devices with thermal interface materials. Energy Rep. 6, 116–122. http://dx.doi.org/10.1016/j.egyr.2019.12.001.

Zhang, X., Zhao, L.-D., 2015. Thermoelectric materials: Energy conversion between heat and electricity. J. Materiomics. 1, 92–105. http://dx.doi.org/10.1016/j.jmat.2015.01.001.

Zhou, J., Yi, Q., Wang, Y., Ye, Z., 2015. Temperature distribution of photovoltaic module based on finite element simulation. Sol. Energy 111, 97–103. http://dx.doi.org/10.1016/j.solener.2014.10.040.

Zhou, J., Zhang, Z., Liu, H., Yi, Q., 2017. Temperature distribution and back sheet role of polycrystalline silicon photovoltaic modules. Appl. Therm. Eng. 111, 1296–1303. http://dx.doi.org/10.1016/j.applthermaleng.2016.10.095.